

## Dissolution arrest and stability of armored bubbles

Manouk Abkarian<sup>1,\*</sup>, Anand Bala Subramaniam<sup>1</sup>, Shin-Hyun Kim<sup>2</sup>, Ryan Larsen<sup>1</sup>, Seung-Man Yang<sup>2</sup>, and Howard A. Stone<sup>1†</sup>

1. Division of Engineering and Applied Sciences, Harvard University, Pierce Hall, 29 Oxford Street, Cambridge, Massachusetts 02138, USA and
2. Center for Integrated Optofluidic Systems and Department of Chemical and Biomolecular Engineering, Korea Advanced Institute of Science and Technology, Daejeon, 305-701, Korea

Dissolving armored bubbles stabilize with nonspherical shapes by jamming the initially Brownian particles adsorbed on their interfaces. In a gas-saturated solution, these shapes are characterized by planar facets or folds for decreasing ratios of the particle to bubble radii. We perform numerical simulations that mimic dissolution, and show that the faceted shape represents a local minimum of energy during volume reduction. This minimum is marked by the vanishing of the Laplace overpressure  $\Delta P$ , which together with the existence of a  $V$ -interval where  $d\Delta P/dV > 0$  guarantees stability against dissolution. The reduction of  $\Delta P$  is due to the saddle-shape deformation of most of the interface which accompanies the reduction in the mean curvature of the interface.

PACS numbers: Valid PACS appear here

Keywords: Armored bubbles, Jamming, Foams, Facets

It is well established that colloidal particles adsorbed on bubble surfaces can increase bubble [1, 2, 3, 4] and foam [5, 6] lifetimes by several orders of magnitude in gas-saturated solutions. This significant increase in stability has potential applications in fields as diverse as biomedicine [7], materials science [8], mineral flotation [9] and food processing [10]. Nevertheless, in spite of the many reports of long-lived foams and bubbles covered with particles (armored bubbles), the mechanism of armored bubble stabilization remains an open question.

In this Letter, we seek to address the issue of stabilization using both experimental and numerical approaches. We begin by considering the dissolution of a single component gas bubble in a liquid saturated with the same gas. The driving force for dissolution is the pressure difference created inside the bubble due to the mean curvature,  $H$  and the surface tension  $\gamma$  that exists at the bubble surface. This Laplace pressure difference,  $\Delta P = 2\gamma H$ , is positive for bubbles, and thus gas in the bubble has a higher chemical potential than the gas dissolved in the liquid. On thermodynamic grounds, dissolution in saturated solutions can be slowed down if this overpressure is reduced or even stopped if the overpressure is eliminated. Indeed, the modest increase in bubble lifetimes for surfactant-coated interfaces is due to the lowering of the gas-liquid surface tension, with more significant increases in lifetime occurring for bubbles covered with gelled monolayers of lipids [11]. However, unlike molecular surfactants or lipids, colloidal particles are not amphiphilic, and thus do not change the surface tension. This then raises the question of how do the adsorbed particles reduce the overpressure of the bubble?

Several related studies provide some insight. Numerical studies of fluid infiltration of granular media have shown a concave deformation of the infiltrating interface

as a function of the volume and contact angle of the particles [12]. A 2D analytical study of armored bubbles found that the “particles” pack into a circular shape, while the interface becomes flat [13] and such a flat interface is stable to perturbations [14]. As we show below, armored bubbles stabilize in various non-spherical and irregular shapes, whose stability can be understood in terms of the interface shapes, characterized by the mean and Gaussian curvatures at the scale of individual particles.

We perform our experiments with negatively charged, surfactant-free fluorescent latex particles (Interfacial Dynamics). Partially coated bubbles were produced as described in [15]. An aqueous sample containing the bubbles was placed on a microscope slide and viewed with an inverted microscope. The small size of the sample ensures that it is saturated with gas. All experiments were carried out at room temperature. The images were acquired with a CCD camera and treated with Image J to obtain a projection of the visible surface of the armored bubble (for details see [16]).

In a typical experiment, the particles adsorbed on a partially covered bubble are dispersed and exhibit thermal motion (Fig. 1A). Occasionally, a few particles form transient aggregates. Analogous equilibrium configurations of colloidal particles on liquid droplets of fixed volume have been observed [17]. In the case of dissolving gas bubbles, the interparticle distances become smaller until Brownian motion is arrested, which we term the interfacial jamming transition. This jammed state can also be reached by packing the bubble surface with colloidal particles in a microfluidic device [18] or by fusing two or more particle-covered bubbles [19]. Once the particle movements have stopped, the bubble does not stabilize but continues to lose gas and deforms away from a spherical shape (Fig. 1A). It is this nonspherical bubble that remains stable, as apparently was first observed by

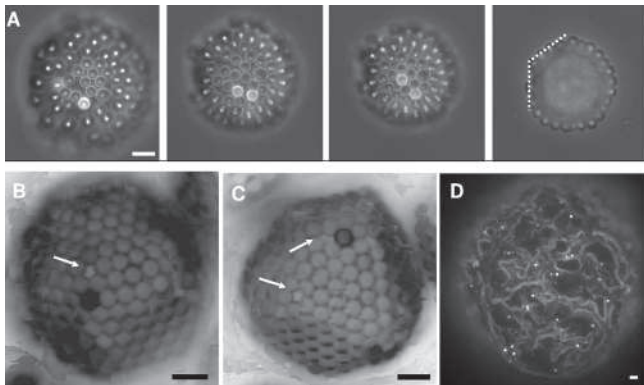


FIG. 1: (A) Dissolution of a partially-covered bubble; 3 s between each frame. Interparticle distances are reduced and the bubble develops planar facets as it stabilizes (white dashed lines). (B-D) Various stable faceted and crumpled shapes of armored bubbles  $a/R$ : (B) 0.22; (C) 0.19; (D) 0.008. The white arrows indicate missing particle defects at the vertices of the bubble. Scale bars  $8 \mu\text{m}$ .

Ramsden [1].

We observe that in an air-saturated solution the final non-spherical shape depends on the ratio of the radius  $a$  of the bead and  $R$  of the bubble. For  $a/R \sim 0.1$ , the bubble exhibits a polyhedral faceted structure (Fig. 1B-C). The intersection of the facets is often a missing particle defect, which represents the position of a five-fold dislocation (white arrows in Fig. 1B and C). The faceting becomes progressively disordered until for  $a/R \ll 0.1$  the bubble appears highly crumpled (Fig. 1D).

The measurement of both the local shape of the air-water interface between the particles and the pressure drop in these micron-size bubbles remains an experimental challenge. A recent numerical approach [20] using Surface Evolver (SE) [21] has shown promise in solving the three-dimensional spherical packing of a small number of particles on emulsion droplets [22]. We perform SE simulations following [20] and report here the evolution of the shape for 122 particles on a bubble surface. We have done additional simulations with almost 400 particles. Solving the full interparticle potential on the surface is computationally expensive, with simulation time scaling as the exponential of the number of particles. Here we use our experimental observations that large-scale rearrangements of the particles are rare to restrict the interparticle potential calculation to nearest neighbors and next nearest neighbors, which makes the simulations with such a large number of particles tractable.

Particles of volume  $V_p$  are modeled as liquid droplets embedded on a larger liquid droplet of volume  $V$ . The particles have a high surface tension (typically 30 times larger than the main liquid-gas surface tension of the bubble) thus maintaining their spherical shape throughout the simulation. Interfacial tensions of the bubble and the particles are chosen to satisfy Young's law at

the solid-liquid contact line and to constrain the contact angle to a fixed value. An exponential repulsive potential is implemented in order to ensure particle non-interpenetrability (see [16]). To approximate the volume reduction that accompanies slow dissolution, the volume  $V$  of the bubble is decreased by 2% increments in each numerical step. SE calculates the equilibrium configuration of the particles and the shape of the gas-liquid surface at each step by minimizing the sum of the gas-liquid surface energies and the total repulsive energy between the particles.

The simulated armored bubble evolves from a spherical shape (Fig. 2A(a)) towards a polyhedral shape with facets as  $V/V_p$  is decreased (Fig. 2A(b)), which matches our experimental observations. Large volume reductions lead to the inward buckling of the facets (Fig. 2A(c)). To quantify this observation further we calculate the asphericity of the bubble [23] which measures the deviation of the shape from that of a perfect sphere. The asphericity is defined as  $\overline{\Delta R^2}/\overline{R^2} = 1/(N\overline{R^2}) \sum_{i=1}^N (R_i - \overline{R})^2$ , where  $N$  is the number of beads,  $R_i$  the distance between the center of the bead  $i$  and the center of mass of all the beads, and  $\overline{R}$  the mean radius defined by  $\overline{R} = 1/N \sum_{i=1}^N R_i$ . We observe a sharp increase of the asphericity when the bubble starts to facet and a significant change of slope when inward buckling is observed (Fig. 2B).

We next calculate the pressure difference  $\Delta P$ , obtained through a native algorithm in SE, between the bubble and its surroundings as a function of  $V/V_p$  (Fig. 2B). Unlike a normal bubble, where  $\Delta P$  is a monotonically increasing function for decreasing  $V/V_p$  (Fig. 2B),  $\Delta P$  of an armored bubble becomes a decreasing function at  $(V/V_p)_{c1}$ , and eventually reaches zero at  $(V/V_p)_{c2}$ . It is significant that these simulations match the experimentally determined shape of the pressure curve of millimeter-size particle-covered oil droplets [24]. Fig. 2B demonstrates the correlation between  $\Delta P$  and the asphericity. Since the particles are held by the interface, this correlation suggests that the interface is being deformed as the volume is decreased. Indeed, the absolute value of the mean curvature  $|H|$  of the gas-liquid interface follows exactly the variation of  $\Delta P$  (except near  $(V/V_p)_{c2}$ , as SE gives only  $|H|$ ). It is thus clear that the vanishing of  $\Delta P$  is due to the decrease of mean curvature of the gas-liquid interface towards zero.

Furthermore, we observe that  $d\Delta P/dV = dP_{bubble}/dV > 0$  at  $(V/V_p)_{c1}$ , which is a requirement for stability [13]. For gas-saturated solutions (the case considered in our experiments),  $\Delta P$  also has to go to zero to ensure mechanical equilibrium. However, more generally chemical potentials must be equal on either side of the interface [25], which can be satisfied with  $\Delta P \neq 0$ . Thus, in the cases of an oversaturated liquid, the bubble may stabilize at various intermediate stages of faceting provided that  $V/V_p < (V/V_p)_{c1}$  (the

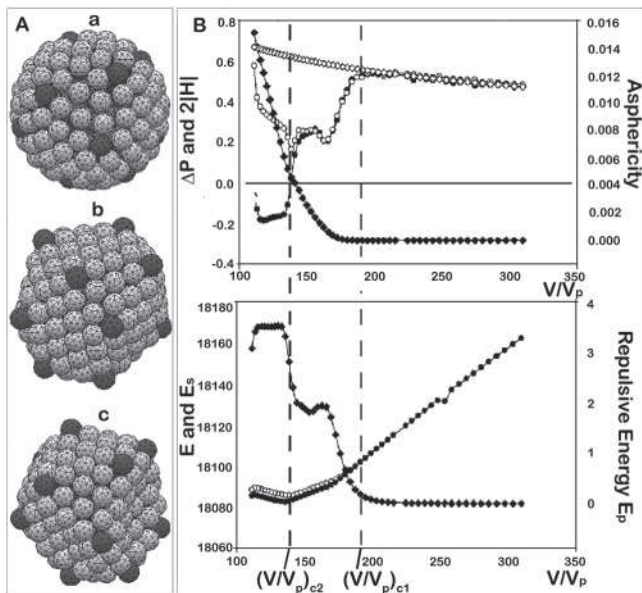


FIG. 2: (A) Bubble shapes obtained for  $V/V_p$  equal to (a) 203, (b) 138 and (c) 120. The darker particles represent five-fold dislocation defects. (B) Top graph. Left vertical axis: ( $\diamond$ )  $\Delta P$  without particles, ( $\bullet$ )  $\Delta P$  with particles and ( $\circ$ )  $2|H|$  versus  $V/V_p$  where  $H$  is the mean curvature. Right vertical axis: ( $\blacklozenge$ ) asphericity versus  $V/V_p$ . Bottom graph. Left vertical axis: ( $\circ$ ) total energy  $E$  and ( $\bullet$ ) the surface energy  $E_S$  of the fluid interface versus  $V/V_p$ . Right vertical axis: ( $\blacklozenge$ ) total repulsive energy  $E_P$  between particles versus  $V/V_p$ .

limit being almost no faceting), while in moderately undersaturated solutions an armored bubble should stabilize with a highly buckled shape. Thus, in principle, the degree of faceting may be used as a probe to determine the degree of saturation of the surrounding medium.

In order to check the stability in terms of energy, we calculate the total energy  $E$ , defined as the sum of the total surface energies  $E_S$  of all of the interfaces and the total repulsive energy  $E_P$  between the particles as a function of  $V/V_p$  (Fig. 2B). All energies are normalized by  $\gamma L^2$ , where  $L$  is defined such that  $L = V_p^{1/3} = (4\pi/3)^{1/3}a$ . For comparison both  $E_S$  and  $E_P$  are plotted in Fig. 2B. We observe that  $E$  and  $E_S$  change slopes as the particles start interacting, reaching a local minimum at the faceted shape when the particle interactions are the highest. Inward buckling of the facets (Fig. 2A(c)) corresponds to a local increase of  $E$  in the energy landscape. Thus, the local minimum is a metastable equilibrium for this system.

The peculiar “kink” that the  $E_P$  curve exhibits during volume reduction (Fig. 2B) can be traced directly to the packing of the particles on the surface of the bubble. As the particles are pushed together during volume reduction, the 12 five-fold defects serve as the vertices of buckling (dark gray particles in Fig. 2A) and are pushed

away from the center of the bubble. The increased distance slightly reduces  $E_P$ . This kink in  $E_P$  also leads to the kink in the  $|H|$  and  $\Delta P$  curves. We suggest that the observations on Fig. 1 B,C of defects associated with missing particles of five-fold coordination could arise from the dewetting and ejection of the particles due to the higher stresses at these points.

It appears that the configuration of the gas-liquid interface is intimately linked to the stability of the armored bubble. We thus sought to characterize the evolution of the gas-liquid interface whose shape can be fully specified by the local variation of the mean curvature  $H$  and the Gaussian curvature  $G$ . Obtaining accurate local numerical values of  $G$  for all simulated  $V/V_p$  through SE proved impossible at the level of refinement of our surface due to numerical errors. Thus, we chose four representative stages in the evolution of the bubble, and systematically refined the triangulation of the interface to reduce numerical noise. The spatial distributions of  $H$  and  $G$  of these surfaces were then determined with Matlab using algorithms proposed for  $H$  [26] and for  $G$  [27]. Representative images of the interface at approximately  $(V/V_p)_{c2}$  are reported in a color-coded scheme in Fig. 3 A,B. Away from the particle contact lines the mean curvature  $H$  is very nearly constant, as expected on thermodynamic grounds, and close to zero;  $G$  has a natural distribution since the Gaussian curvature need not be constant.

Despite the high level of refinement, it is apparent that there is still some dispersion in  $H$  (and in  $G$  as well), whose origins are (i) difficulty in numerical calculations near contact lines and (ii) errors associated with the triangulation valence around the vertices which can be amplified during the determination of  $G$  [28]. Nevertheless, we can draw some conclusions about the global evolution of the surface curvatures. Indeed, a pair of values  $(H_i, G_i)$  is associated for each vertex defining the interface. To characterize the global nature of the interface, we calculate the number density of vertices whose curvatures range  $[H, H + 0.03]$  and  $[G, G + 0.03]$ . We report on Fig. 3C-F the plot of the contour map of this binning of the  $H - G$  space; shading corresponds to the number density of points. As a guide, a sphere would correspond to a parabola ( $G = H^2$ ) in these plots and the origin  $(0, 0)$  corresponds to a planar interface. For large  $V/V_p$ , when the particles are not interacting, the distribution of points is concentrated on the parabola, where both  $H$  and  $G$  are positive (Fig. 3C). Then, for decreasing values of  $V/V_p$ , the center of the distribution shift towards zero in the  $H$ -direction, while in the  $G$ -direction it becomes negative. These results indicate a saddle-shape deformation of much of the interface as the volume is reduced.

We interpret the inward curvature of the interface as a consequence of Newton’s third law. The repulsive beads produce an outward normal force on each other, because of their confinement on a closed spherical surface. This outward force must be balanced by an inward saddle-

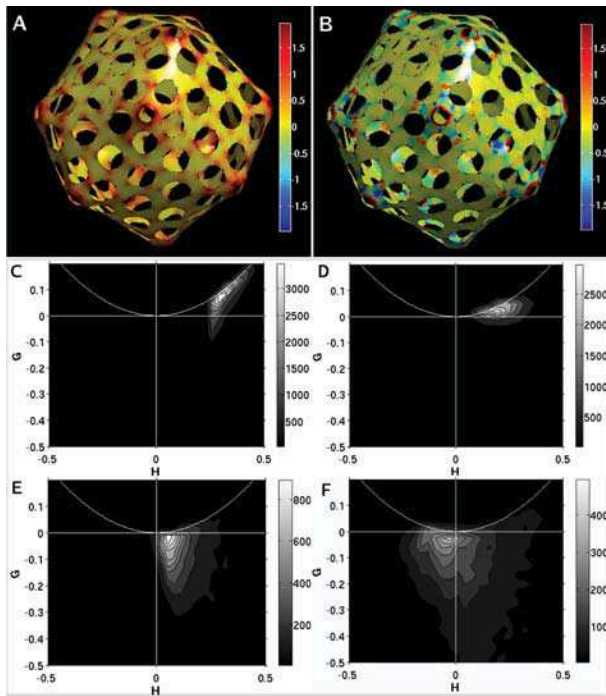


FIG. 3: Interfacial distributions of (A) the mean curvature  $H$  and (B) the Gaussian curvature  $G$ , for  $V/V_p$  138.1 close to  $(V/V_p)_{c2}$ . 2D histogram of the number of vertices of the interface whose curvatures range between  $[H, H+0.03]$  and  $[G, G+0.03]$  obtained for  $V/V_p =$  (C) 253, (D) 162.3, (E) 138.1 and (F) 117.5. Total number of vertices 63016.

shaped deformation of the fluid-fluid interface. This reactive deformation of the interface, which is required for mechanical equilibrium at each volume reduction, leads to a reduction in the Laplace pressure. We emphasize that this saddle-shaped deformation should appear on any initially spherical fluid-fluid interface carrying repulsive particles, as soon as the particles are close enough to interact. The details of the interparticle repulsive force is not relevant for this argument, the limiting case being the case of a hard sphere repulsion between the particles, where the interface will deviate from its spherical shape only when the particles enter into contact.

In conclusion, we have shown that armored bubbles stabilize in faceted or crumpled shapes by jamming the particles on their interfaces. Through simulations we demonstrated that the faceted state is a minimum energy configuration characterized by a mostly saddle-shaped gas-liquid interface with zero mean curvature. This minimum is also marked by the vanishing of the Laplace overpressure  $\Delta P$ , and  $d\Delta P/dV > 0$  which guarantees stability against dissolution. The results we obtained in this study should also be applicable to describe the interface and behavior of liquid-liquid systems.

We thank the Harvard MRSEC (DMR-0213805) and Unilever Research for support and D. Gregory for helpful conversations. SHK and SMY were supported by the

Creative Research Initiative Program of MOST/KOSEF and the BK21 program. We thank E. Lauga for help with SE.

\* Present address: Laboratoire des Colloïdes, Verres et Nanomatériaux, UMR5587, CC26, UMII, 34095 Montpellier Cedex 5, France; Electronic address: abkarian@lcvn.univ-montp2.fr

† Electronic address: has@deas.harvard.edu

- [1] W. Ramsden, Proc. R. Soc. London **72**, 156 (1903).
- [2] B. Johnson and R. Cooke, Science **213**, 209 (1981).
- [3] Z. Du, M. Bilbao-Montoya, B. Binks, E. Dickinson, R. Ettelaie, and B. Murray, Langmuir **19**, 3106 (2003).
- [4] E. Dickinson, R. Ettelaie, T. Kostakis, and B. Murray, Langmuir **20**, 8517 (2004).
- [5] R. Alargova, D. Warhadpande, V. Paunov, and O. Velev, Langmuir **20**, 10371 (2004).
- [6] B. Binks and T. Horozov, Angew. Chem. **44**, 3722 (2005).
- [7] E. Schutt, D. Klein, R. Mattrey, and J. Reiss, Angew. Chem. **42**, 3218 (2003).
- [8] P. Krachelsvky and K. Nagayama (Elsevier Science, New York, 2001).
- [9] A. Adamson and A. Gast (Wiley-Interscience, New York, 1997), 6th ed.
- [10] B. Gibbs, S. K. I. Alli, and C. Mulligan, Int. J. Food Sci. Nutr. **50**, 213 (1999).
- [11] P. B. Duncan and D. Needham, Langmuir **20**, 2567 (2004).
- [12] J. Hilden and K. Trumble, J. Colloid Interface Sci. **267**, 463 (2003).
- [13] S. Kam and W. Rossen, J. Colloid Interface Sci. **213**, 329 (1999).
- [14] R. Subramanian, R. Larsen, and H. Stone, Langmuir **21**, 4526 (2005).
- [15] A. B. Subramanian, C. Méjean, M. Abkarian, and H. Stone, Langmuir **22**, 5986 (2006).
- [16] EPAPS supplementary information.
- [17] A. Bausch, M. Bowick, A. Cacciuto, A. Dinsmore, M. Hsu, D. Nelson, M. Nikolaidis, A. Travesset, and D. Weitz, Science **299**, 1716 (2003).
- [18] A. B. Subramanian, M. Abkarian, and H. Stone, Nat. Mat. **4**, 553 (2005).
- [19] A. B. Subramanian, M. Abkarian, L. Mahadevan, and H. Stone, Nature **438**, 930 (2005).
- [20] E. Lauga and M. Brenner, Phys. Rev. Lett. **93**, 238301 (2004).
- [21] K. Brakke, Exp. Math. **1**, 141 (1992).
- [22] V. Manoharan, M. Elsesser, and D. Pine, Science **301**, 483 (2003).
- [23] J. Lidmar, L. Mirny, and D. Nelson, Phys. Rev. E **68**, 051910 (2003).
- [24] H. Xu, S. Melle, K. Golemanov, and G. Fuller, Langmuir **21**, 10016 (2005).
- [25] E. Guggenheim (North-Holland, Elsevier, Amsterdam, 1967), 4th ed.
- [26] M. Meyer, M. Desbrun, P. Schroder, and A. Barr, in *International workshop on visualization and mathematics* (Berlin-Dahlem, Germany, 2002).
- [27] J. Goldfeather and V. Interrante, ACM Trans. Graph. **23**, 45 (2004).

- [28] V. Borrelli, F. Cazals, and J.-M. Morvan, *Comput. Aided Geom. Design* **20**, 1 (2003).